On the construction of an experimental setup for detection of cerium in Y_2SiO_5

Master's thesis
by
Johan Tholén

Lund Reports on Atomic Physics, LRAP-370
Lund, December 2006

Abstract

In this thesis the first steps on the construction of an experimental setup for detection of cerium (Ce) doped into an YSO crystal are taken. The setup will be used to find and characterize the zero-phonon-line (ZPL) between the 4f and 5d levels in Ce. In the long-term, this information is important since it could answer if the ZPL in Ce is suitable to use in a single-ion readout scheme, designed to make single-instance quantum computing in rare-earth-ion-doped crystals possible.

The results presented in this thesis are concerned mainly with an external cavity diode laser (ECDL) with a centre wavelength of 372.1 nm at $T = 25°\mathrm{C}$. A good coupling between the laser diode and the external cavity has been achieved, indicated by a reduction of laser threshold current by approximately 12 %. Attempts to resolve the mode structure of the laser light from the ECDL have been made and these indicate that the ECDL is operating in single-mode. Wavelength measurements have also been made and the report contains suggestions on how to simplify this process. The scan-width accomplished by means of rotating the grating in the ECDL seems to be sufficient to reach the expected ZPL wavelength, which is thought to be located at 370.7 nm. The report also contains an appendix where the procedure used to align the ECDL is outlined.

Populärvetenskaplig sammanfattning

I takt med att våra datorer har blivit snabbare och bättre så har deras kretsar blivit mindre och mindre och komponenterna i dessa kretsar börjar snart närma sig storleken av ett fåtal atomer. Fysik på atomära nivåer skiljer sig från den fysik vi är vana vid att använda för att beskriva uppförandet hos våra makroskopiska vardagsföremål. För att förklara beteenden på denna skala används kvantmekanik. Enligt kvantmekaniken kan atomära system befinna sig i flera tillstånd samtidigt, i en så kallad *superposition*. När man försöker undersöka tillståndet hos ett kvantmekaniskt system så reduceras det till ett av sina möjliga tillstånd. Man kan därför inte direkt undersöka ett sådant system utan att påverka det. Det finns flera andra kvantmekaniska effekter, t.ex. möjligheten att en mätning på en partikel ögonblickligen kan påverka tillståndet hos en annan partikel över stora avstånd, s.k. sammanflätning. En typ av dator som syftar till att utnyttja de kvantmekaniska fenomenen till sin fördel är *kvantdatorn*. Den använder sig av möjligheten att använda superpositioner för att lagra information i så kallade *kvantbitar*, den kvantmekaniska motsvarigheten till den klassiska datorns *bitar*. En samling kvantbitar kan representera flera olika tal samtidigt, till skillnad från en samling bitar som bara kan representera ett tal åt gången. Genom att utföra listiga operationer på en samling kvantbitar kan beräkningar, som i vanliga datorer kräver flera steg, utföras parallellt med ett enda steg.

Kvantinformationsgruppen på Lunds Tekniska Högskola använder kristaller innehållande jonslag som kan användas som kvantbitar för att skapa en kvantdator. För att utföra beräkningar och läsa ut resultat skickas laserpulser in i kristallen. Kvantbitarna tar upp energin från ljuset för en kort stund varefter de återgår till sitt ursprungliga tillstånd och gör sig av med sin överskottsenergi genom att sända ut ljus. Genom att göra noggranna mätningar av det utsända ljuset kan resultaten från beräkningarna läsas ut. Jonerna som utgör kvantbitarna är väldigt stabila, detta för att kvantdatorn ska hinna göra många operationer innan deras tillstånd förstörs av störningar från omvärlden, t.ex. termiska vibrationer. Denna stabilitet innebär bland annat att de sänder ut väldigt lite ljus när de gör sig av med sin

överskottsenergi. Det är svårt att göra noggranna mätningar på svagt ljus, därför man hittills använt flera parallella kvantdatorer. Varje kvantdator sänder ut ljus som svar på de inskickade ljuspulserna. Är antalet kvantdatorer tillräckligt stort blir det lättare att detektera ljuset.

Det finns dock ett problem med att använda flera kvantdatorer. För att kunna göra beräkningar på stora tal måste också antalet kvantbitar vara stort. Beräkningar har visat att när antalet kvantbitar ökar så minskar antalet tillgängliga kvantdatorer i kristallen. Om däremot enbart ljuset från en ensam kvantdator kunde detekteras skulle det vara lättare att lägga till många kvantbitar. För att göra detta möjligt är idén att introducera ytterligare en typ av jon i kristallen. Denna jon ska ha egenskapen att sända ut mycket ljus när den gör sig av med överskottsenergin från de inskickade ljuspulserna. Genom att låta den här *utläsningsjonen* befinna sig väldigt nära någon av kvantbitarna i kristallen så kommer kvantbitarnas tillstånd påverka ljuset som emitteras av utläsningsjonen. Genom att skicka in många ljuspulser i följd kan signalen från utläsningsjonen mätas många gånger för att få ett noggrannt värde.

I det här examensarbetet har de första stegen tagits mot att konstruera en mätuppställning som kan användas för att undersöka om en cerium-jon verkar ha de lämpliga utläsningsegenskaperna. Arbetet har varit mer tidskrävande än väntat så inga mätningar på jonen har hunnits med. Den mesta tiden har istället lagts på att testa utrustningen och få den att fungera. Särskilt mycket tid har lagts på att jobba med en s.k. extern-kavitet-diodlaser och mäta dess våglängd. Denna laser förväntas vara mycket praktisk vid de planerade mätningarna.

Contents

Introduction

Background

Quantum computing is currently a very active field of research. Much of the attention and excitement around the subject is spurred by indications that quantum computers are able to solve some certain computational problems much more efficiently than classical computers. There is also a more fundamental interest towards using quantum mechanical systems to process and store information which has implications on our understanding of what information is and how Nature works at its most fundamental level. Much effort is directed towards finding physical systems that could be used to implement a quantum computer. There are many different suggestions on how to do this, but what all designs have in common is the ability to implement qubits.

The qubit is the basic building block for a quantum computer, analogous to the bit in the classical computer. There are however large differences between the two *information atoms* in the sense that a collection of qubits (a register) can be set up to store several values at the same time by using the quantum mechanical property of superposition, whereas a collection of bits only can store one value at a time. Using qubits, quantum computer algorithms can be constructed that can perform several computations and operations in parallel. To be able to do calculations that are interesting in practice, the quantum computer must have a large number of qubits. This is a major obstacle in all quantum computer implementations. Today, it is unknown if it ever will be possible to construct large-scale quantum computers. The research is still very important since all attempts of realizing quantum computers involves manipulation and investigation of physical systems on scales where quantum mechanics sets the rules. This gives many opportunities to investigate and confirm quantum mechanical properties as well as to increase one's knowledge about how to control the world on the smallest scale.

The Quantum Information Group in Lund are using rare-earth-ion-doped crystals to implement the qubits and lasers to perform the operations and reading out the results. To facilitate readout of the information stored in the qubits, many quantum computers instances are used in parallel. One of the

disadvantages with this so-called ensemble quantum computer is that it does not scale very well. Adding more qubits to the quantum computers decreases the number of usable quantum computer instances in the crystal. If instead a single quantum computer instance could be used and readout, it would be easier to add further qubits to the register. The single-instance approach however requires the capability to detect single ions. One way to facilitate single-ion detection could be to co-dope the rare-earth-ion-doped crystal with another rare-earth-ion species. This new ion should have properties that makes it easier to detect spectroscopically than the ions used as qubits. Cerium (Ce) has been suggested as a suitable readout ion, but many of its properties needs to be measured before anything conclusive can be said about this.

The diploma work

The aim of this diploma work was to construct an experimental setup that could be used to locate and characterize the ZPL in Ce. Setting up the equipment proved to be more time-consuming than expected, therefore the setup couldn't be put into use. This thesis is written with the hope that it will be useful and time-saving to anyone continuing on this project.

The text is divided into a theory section, chapter 1 through 2 where some background to different concepts relevant for this thesis are covered, such as quantum computing and the single-instance readout scheme. In chapter 3 a somewhat lengthy discussion is given concerning the external cavity diode laser (ECDL) which was a major component in the planned experiments. In chapter 4 the experimental setups are discussed. This is followed by the results in chapter 5 and the conclusions in chapter 6. There are also two appendices, the first is an instruction on how to operate and align the ECDL and the second gives a brief description on how to mix the Pyridine-2 dye used in the dye laser.

Chapter 1

Quantum computing

In this chapter an introduction to the field of quantum computing will be given. Given the scope of this field this overview will barely scrape the surface of the theory and concepts. The interested reader is recommended to have a look at [1].

1.1 General

To be able to get a sense of what quantum computing is about, it is good to know what is meant by the *efficiency* of an algorithm, or the *complexity* of a computational problem. Imagine some general data set consisting of N elements. A very simple algorithm could be to go through this set of elements and check the value of each element. This would require the same operation to be performed on every element in the set. The time to check every single element is assumed to be constant, say c. This gives the total time for the algorithm

$$t(N) = cN. \tag{1.1}$$

So the time to perform the entire operation depends linearly on the number of elements in the data set. When different algorithms are compared in terms of performance, the constant c is usually ignored and the time complexity of the algorithm is stated to be linear. Imagine two different algorithms giving the same result where the first has a time complexity of N and the second one has a time complexity of N^2. Given an increase in the size of the data set by a factor of 10, the first algorithm will take 10 times longer to run to an end but the second algorithm will take 10^2 times longer. In general, a polynomial time complexity is considered to be very good. For many problems the time complexity can be exponential or even worse. These problems are considered not to be possible to solve in an efficient way.

The computers of today work in the way just described. Going through data sets sequentially, performing operations that can be described in an algorithmic way. This is known as the *Turing-model* of computation. It

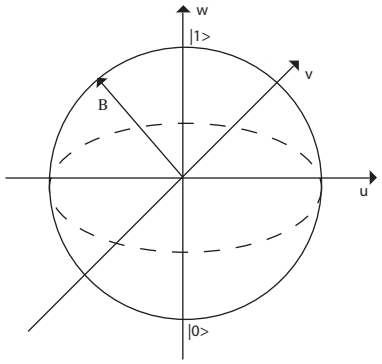

Figure 1.1: The Bloch-sphere showing the population inversion along the w-axis and the complex polarization in the uv-plane. The qubit state $|1>$ is chosen as the excited state and the $|0>$ corresponds to the ground state. The vector $B(u, v, w)$ is called the Bloch-vector and shows the state of the two-level system.

was long thought that this was the most general way of computing and that any other model of computation could be simulated efficiently (in terms of time complexity) on a Turing-machine. It was also thought that the actual physical implementation of the computer was irrelevant in terms of efficiency. However in 1982 Richard Feynman showed that quantum mechanical systems not could be simulated efficiently on a classical computer and suggested that a computer based on quantum mechanical systems could do this in an efficient way [2]. This was followed by David Deutsch who in 1985 investigated if a new kind of computer could be constructed that could efficiently simulate any physical system [3]. Today it is still unknown if the model proposed by Deutsch is sufficient to do this ([1], page 6).

1.1.1 Qubit

Whereas in a classical computer the information is stored in bits, where each bit can have the value of either 0 or 1, in a quantum computer information is stored in qubits - a quantum mechanical system with two states denoted $|0>$ and $|1>$. According to quantum mechanics this qubit can be in an arbitrary superposition of these states $\alpha|0> + \beta|1>$. The state of the qubit is conveniently depicted in the Bloch-sphere where $w = |\beta|^2 - |\alpha|^2$ and the uv-plane describes the phase of the superposition relative to the phase of a driving electromagnetic field, see figure 1.1. Since there are infinitely many points on the Bloch-sphere it may seem like an infinite amount of information could be coded into a single qubit. However, to extract information from the qubit a measurement has to be done and the qubit will then collapse to

either the $|0>$ state or the $|1>$ state. To map out the exact position of the Bloch-vector infinitely many measurements needs to be performed and a single qubit can thus not be used to store more information than a classical bit. However if some other operation that doesn't extract information is applied to the qubit the system will evolve in a coherent way. During this evolution, Nature keeps track of all the information of the qubit state. So in a way, it is this concealed information processing that quantum computers use.

A collection of qubits is called the quantum computer register analogous to the register of a classical computer. An n-bit classical computer register can store 2^n different values. An n-bit quantum register on the other hand can hold 2^n different values at the same time. As an example, consider a 2-bit qubit register. Since the qubits can be but in an arbitrary superposition of states the register is

$$\alpha_{00}|00> +\alpha_{10}|10> +\alpha_{01}|01> +\alpha_{11}|11> \tag{1.2}$$

where $|ij>$ is a shorthand for $|i>_{qubit\,A}\ |j>_{qubit\,B}$ and the probability amplitudes satisfy $\sum_{i,j} |\alpha_{i,j}|^2 = 1$. Applying some operation to this state will manipulate all four states at the same time. This is a simple example of quantum parallelism.

1.2 Gate operations

Looking at the Bloch-sphere description of the qubit an infinite number of single qubit operations can be imagined (i.e. rotations of the Bloch-vector by some arbitrary angle). There are also a large number of multiple-qubit quantum gates. If the instruction set of a quantum computer is to be complete it has to be able to perform many different kinds of single- and multiple-qubit gates. The *universality theorem* makes this much easier since it states that *"any logic quantum gate can be implemented by using a combination of a 2-qubit gate and single qubit gates"*. It can also be shown that all single qubit gates can be broken down into a product of two rotation operations for some fixed set of angles.

One of the 2-qubit gates that can be used in an universal quantum computer is the controlled-NOT gate. The classical 2-bit controlled-NOT or CNOT flips the value of the *target* bit depending on the state of the *control* bit according to this table.

control qubit	*target qubit*	*result*
0	0	0
0	1	1
1	0	1
1	1	0

For a general 2-qubit state the quantum CNOT can not be summarized in such a short way, but if both the target- and control-qubit start out in one of their basis states the results of the classical and quantum mechanical CNOT coincide.

1.2.1 Algorithms

Though it is still not well understood why or if quantum computers are more powerful than classical computers, a few quantum computer algorithms have been constructed that are superior to any known classical algorithm solving the same problem. One is Shor's factorization algorithm [4] which factorizes a given integer into its prime factors. This is a very important problem since prime factorization is the foundation on which one of the more commonly used cryptography schemes relies. Another major algorithm is Grover's search algorithm [5] that searches for a given element in an unstructured set. This algorithm has a $\sqrt{n}$ advantage in time complexity compared to the most efficient algorithm known for classical computers.

1.3 Implementations

Many different physical systems have been proposed as hardware for quantum computers, ion traps, high-Q cavities, solid-state systems, rare-earth-ion-doped crystals to name only a few. The actual implementations of these systems differs a lot but they all rely on the concept of having some quantum mechanical system constituting the qubits that can be controlled in a well-defined way. The system has to be shielded from the surrounding world in a way that minimizes interactions between the qubit registers and the environment for a time at least as long as the time required to perform the required operations of the algorithm and readout the result. In other words, the system must have a sufficiently long coherence time. This is a major design criterion and for the implementations mentioned above they vary by many orders of magnitude.

One major obstacle that no implementations yet have overcome is that of scaling. For a quantum computer to do anything useful in practice the number of qubits has to be large, so far the largest qubit register created consisted of 12 qubits, [6]. One of the reasons why it is difficult to increase the number of qubits could be that increasing the size of the system also increases the probability to have interactions with the surroundings, which in turn decreases the coherence time of the qubits. Scaling is also a problem with the approach used by the Quantum Information Group in their quantum computer approach.

Chapter 2

Rare earth quantum computing

In this chapter, the implementation pursued by the Quantum Information Group at Lund Institute of Technology will be described briefly, i.e. the creation of the qubits and how to implement gates. Th scaling performance for the so-called multiple- and single-instance quantum computer will also be discussed as well as how to use cerium as readout ions in single-instance quantum computing.

2.1 Creating the qubit

The material used is an *yttrium-oxy-ortho-silicate* crystal, Y_2SiO_5 (or more conveniently YSO). The crystal is doped with *rare-earth* atoms or *lanthanides* that replaces some of the Y-ions in the crystal lattice. The lanthanide series has the electronic configuration $5s^2 5p^6 4f^n 5d^m 6s^2$, where $1 \leq n \leq 13$ and m is either 1 or 0. Binding to the YSO-crystal the lanthanide will loose the $5d^1$ and $6s^2$ electrons and become a trivalent ion (Re^{3+}) with a partially filled $4f^n$ shell relatively well shielded from the surrounding electric field in the crystal. This allows the electronic structure of the Re^{3+} in the crystal to be approximately described by the free ion model. For low temperatures the vibrations in the crystal will be small and the position of the ions will be fixed so the Re^{3+} ions will behave almost as a Doppler-free gas.

Praesodynium (Pr) is a lanthanide that has suitable properties for being used as a qubit. In figure 2.1 the ground state and first excited state of the free Pr^{3+} ion is shown. Both the ground state and the excited state is split up into three two-fold degenerate second-order hyperfine structures. The transitions between the ground state hyperfine levels will be very weak so the lifetime of the hyperfine states in the ground state will be on the order of 100 s for Pr. The linewidths of the transition between the ground states and the excited states (Γ_h) are on the order of kHz. The $|0\rangle$ and $|1\rangle$ states are chosen as the qubit levels and the $|e\rangle$ state is used to coherently

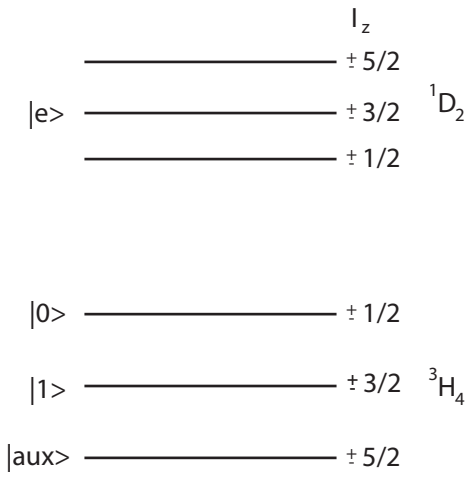

Figure 2.1: Level structure of the ground and first excited state of the free Pr^{3+} ion. The states labelled $|0>$ and $|1>$ are used as the qubit levels, $|e>$ is the excited level used when coherently driving the electron between the qubit states and $|aux>$ is used to hold ions that are not suitable to use as qubits.

drive transitions between the qubit levels[1] using laser pulses. In $|aux>$ the ions that absorb at the qubit frequency but still aren't suitable as qubits are stored. Since the crystal lattice isn't perfect, every Pr^{3+} ion will sit in a slightly different environment and thus experience a slightly different surrounding electric field. This will lead to an inhomogeneous spread (Γ_{ih}) of the energy splitting between the ground state $4f^2$ and the excited state 5d. The $4f^2$ level isn't as sensitive to changes in the crystal field so the hyperfine splitting in the ground state will not vary much between different ions[2]. For a suitable doping concentration (typically 0.005-0.1 %) this results in a broad inhomogeneous profile of the order of GHz, see [7], with a large number of addressable frequency channels Γ_{ih}/Γ_h. This is illustrated in figure 2.2. By using spectroscopic hole-burning techniques a broad spectral region is vacated and by re-pumping, a narrow peak of ions (a frequency channel) can be created in the centre of the pit, see figure 2.3, allowing excitation of these ions while leaving all other ions unaffected. The peak now constitutes an ensemble of equivalent qubits.

[1] In NMR the same scheme is employed except that the transition between the qubit levels is directly driven by using a rf-field. It is however advantageous to use an optical field since it is then possible to drive the transition more quickly.

[2] In practice however this also needs to be taken into account.

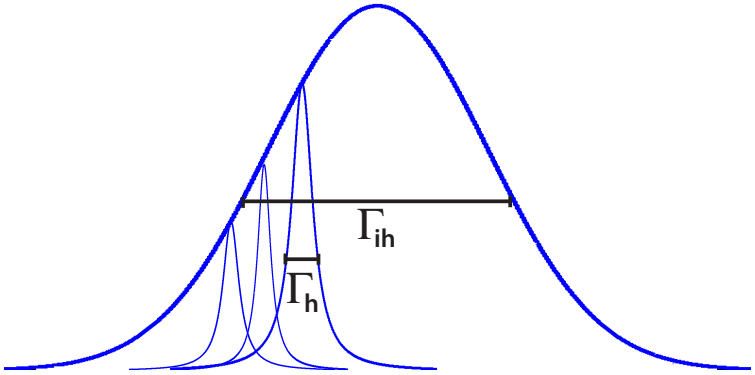

Figure 2.2: Illustration of the broad inhomogeneous absorption profile of the $4f \leftrightarrow 5d$ transition and three narrow frequency channels.

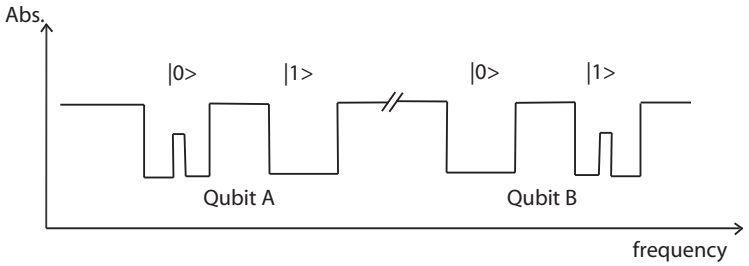

Figure 2.3: Enlarged section of the inhomogeneously broadened absorption profile around two qubit structures. The peaks consists of a large number of ions.

2.2 Implementing gates

To be able to do anything useful with the qubits some mechanism to implement gates has to be available. As mentioned in the general discussion about quantum computers the CNOT operation is a very useful gate operation. Only the 2-qubit CNOT will be considered here but the n-qubit CNOT can be implemented in a similar fashion. Because of the electric field from the crystal the qubit ions have a permanent dipole moment when in the ground state. Excitation will change the electronic distribution around the ion and therefore also change its dipole moment, leading to an altered electric field in the vicinity of the ion. For ions situated close enough to each other this electric field will be large enough to shift the optical transition ($|0> \leftrightarrow |e>$ or $|1> \leftrightarrow |e>$) out of resonance. Assuming that the qubits A and B seen in figure 2.3 only consists of ions that are situated so close relative to one another that the dipole-dipole interaction is sufficiently large

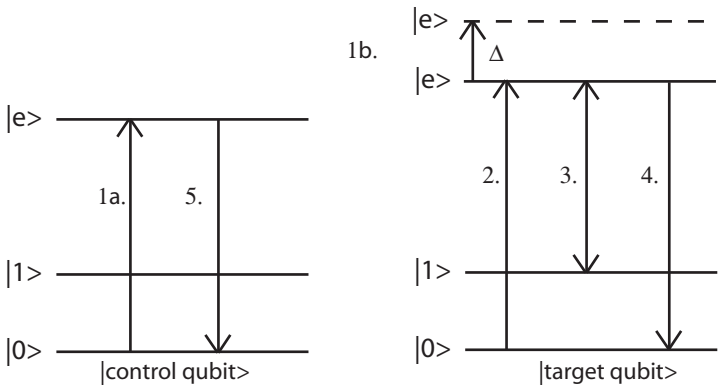

Figure 2.4: Implementation of the 2-qubit CNOT operation. The dipole-dipole shift Δ is only induced if the control qubit is starting in the $|0>$ state. The shift will bring the target qubit out of resonance with the incident laser pulses in step 2, 3 and 4.

to shift the other qubits out of the pit[3], the 2-qubit CNOT operation can be implemented according to figure 2.4.

2.3 Scalability problems

In the description of the CNOT gate it was assumed that the qubit ions are situated so close to all other qubit ions in the register that the dipole-dipole interaction is sufficiently large to be able to control all other qubits in the register. If it is assumed that the probability p to find two qubits mutually controlling each other in all quantum computer instances and that p is independent of the number of qubits already in the register, the probability to construct an N-bit register is $P = p^{N-1}$. For P to be reasonably large p has to be approximately 1, but this is far from the case in the crystals used, since the doping concentration is fairly small. So increasing the register size will quickly decrease the number of quantum computer instances available in the crystal. One immediate solution to this scaling problem would be to use higher doping concentrations or to use ions with larger difference in dipole moment. Larger interactions between the ions and the crystal lattice results in a larger inhomogeneous width which in fact has a decreasing effect on the number of available ions per frequency channel. Large interaction distances increases the chance to find qubit ions that can control each other mutually which improves the scaling performance but it also increases the probability that equivalent qubit ions in different quantum computer instances will start to affect each other. Promoting one of the qubits (A) to the excited state

[3]This can be accomplished by certain pump-schemes

will shift the other qubit (B) out of resonance. But exciting A will also mean that B can be excited which will then shift A out of resonance. This render the light pulses less effective in exciting the qubits[4], a phenomena known as the dipole-dipole-blockade. This problem can be solved by burning away those ions to the $|aux>$. Pulse schemes to do this and thus improving the scalability for the multiple-instance quantum computer have been suggested by [8], but this further increases the demands of stability of the system.

A better solution would be to use bus-ions. If instead of requiring that all ions in the register can control each other directly a central bus-ion can be used to mediate the interaction between ions. Without the bus-ion all communicating ions must be situated within a sphere of radius r, but with the bus-ion the radius is increased by a factor of 2, increasing the interacting volume by $2^3 = 8$. The use of a central ion also offers other advantages such as the ability to connect to other bus-ions thus connecting different branches of communicating ions with each other. To achieve the best scaling possibilities though, the direction to move seems to be towards a single-instance quantum computer. Every ion is surrounded by a number of ions that can mutually control each other. All of these ions in turn has other neighbours which also can control each other. This constitutes a whole chain of interacting ion groups. The difference from the former approaches is that each qubit now only is represented by one ion, thus requiring single-ion detection to be able to make a readout. The details of both bus-ions and the single-instance scheme are discussed in much more detail in [8].

2.3.1 Single-instance and multiple-instance quantum computer

In a single-instance quantum computer the physical system harbouring the quantum computer only contains one instance of every qubit in the register. The pulses that are needed to coherently drive the qubits can be simplified compared to the multiple-instance case where the inhomogeneous broadening of the hyperfine structure in the ground state and also on the optical transition has to be taken into account. Another difference between the two implementations is the readout signal, in a single instance quantum computer the quantum register will collapse to one of the possible results. This is in contrast to the multiple-instance implementation where upon readout all the instances will collapse into different states turning the readout signal into an average of all possible results, i.e. basis states. This signal will be easier to detect than a signal from only a single qubit but it can be more difficult to interpret. The problem with the single instance quantum computer is that it requires the possibility to detect individual ions. In the following section one technique to make this possible will be described.

[4]The Rabi-frequency will decrease by 50 %.

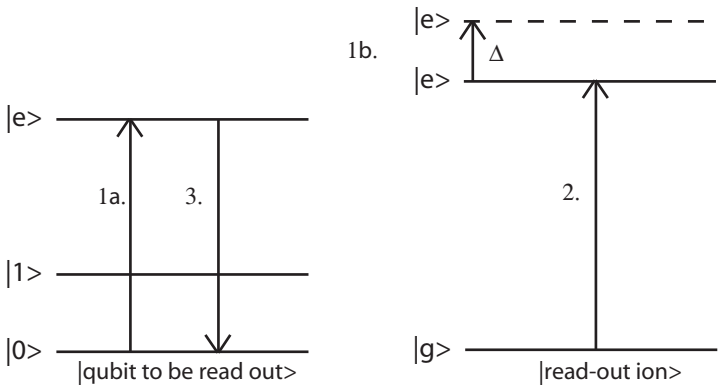

Figure 2.5: The readout process for detecting the state of a single qubit. The shift in 1b brings the readout transition out of resonance with pulse 2 so no fluorescence will be observed from the readout ion if the qubit starts in the |0> state. If the qubit starts in the |1> on the other hand the readout ion will be promoted to the excited state and after some short time relax back to the ground state while emitting fluorescence light.

2.4 System for single-ion detection

The idea proposed is to co-dope the crystal very lightly with another rare-earth-ion that has properties that makes it easier to detect spectroscopically than the qubit ions. The readout process could work in a way very similar to the CNOT operation, see figure 2.5. The readout transition can be cycled many times until a good detection signal has been accumulated.

As mentioned previously, the qubit ions have very small homogeneous linewidths and in turn very long lifetimes. Since the number of photons that can be emitted per unit time from an atom at a given transition is inversely proportional to the lifetime of that transition, the qubit ions will emit a very small number of photons.[5] A good readout ion should thus have the following properties.

1. It should have a transition with a frequency different from the qubit frequencies so that the readout light doesn't affect the state of the quantum register.

2. The readout transition should be able to be taken out of resonance through the dipole-dipole interaction by at least one of the qubits in the register.

[5]If fluorescence detection is used to detect the ions the photons will be emitted in random directions making it even more difficult to detect the qubit.

3. The readout transition shouldn't be shifted into any of the qubit frequencies.

4. Introducing the readout ion in the crystal shouldn't change the properties of the qubit ions.

5. The lifetime of the readout transition should be as small as possible to give as high a photon yield as possible. This means that it should be possible to cycle the transition many times on the timescale of the excited state lifetime of the qubit ions.

6. To be able to cycle the transition many times the valence electron should have a very small probability to be caught in a non-fluorescent state, making the readout process impossible.

In [8] an explanation on how to find the qubits and readout ion is given.

2.5 Ce^{3+} as readout ion

Looking for a readout ion, Ce^{3+} was suggested as the most suitable candidate. Some spectroscopy on Ce^{3+} has already been done but this has been in other inorganic compounds than YSO, see [9]. Although no specific conclusions about the properties of Ce^{3+}:YSO can be drawn from these studies it is interesting to note the existence of a so-called zero-phonon-line (ZPL) when Ce^{3+} is doped into some crystals. For more details on the following subjects, see [10].

2.5.1 The level structure of Ce^{3+}

When cerium, which is a rare earth element, is doped into an YSO crystal it becomes a trivalent ion with one valence electron in the 4f level. As described in the beginning of this chapter three electrons from the $5d^16s^2$ participates in the binding to the crystal, leaving one valence electron in $4f^1$ relatively well shielded from the surrounding crystal field, so the free ion spectrum serves as a useful approximation. The level structure is described by the LS-coupling scheme which gives the ground state terms $^2F_{5/2}$ and $^2F_{7/2}$. The first excited state 5d consists of the terms $^2D_{3/2}$ and $^2D_{5/2}$. In the YSO lattice the ion is subjected to the surrounding crystal field and the terms get further split up because of the Stark interactions. There is also some mixing of the terms, especially for the excited state.

2.5.2 The zero-phonon-line

The vibrations of the surrounding crystal influences the electronic transitions in Ce^{3+}. The vibrations of the crystal lattice can be modelled using coupled

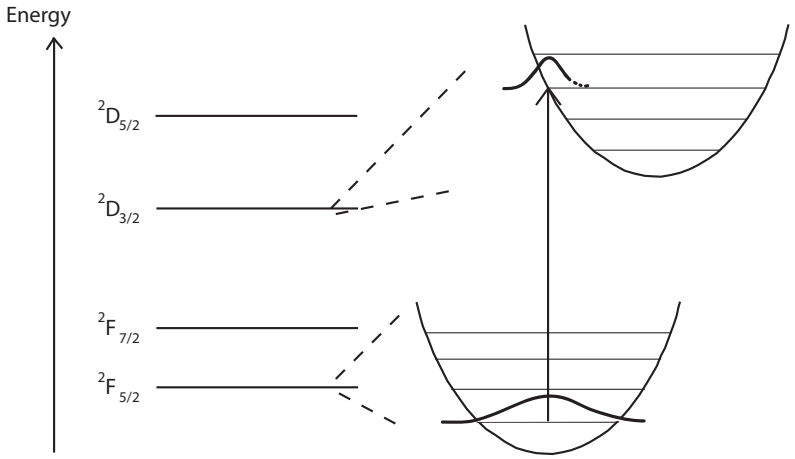

Figure 2.6: Simplified level-scheme for Ce^{3+}. The vibrational structure of two of the levels is also illustrated. A large horizontal displacement between the two parabolas corresponds to a large S-parameter and for $S = 0$ the two parabolas would be on top of each other.

harmonic oscillators. The energies of the lattice vibrations are discrete and these energy quantas are called phonons. At low temperatures only few phonons are present in the crystal. The electronic wave functions both affect and become affected by the phonons. This can be understood in a simple picture. The ions in the crystal can be imagined to be coupled to each other by springs with some spring constant k. Changing the electronic distribution around an ion will change the surrounding electric field and will thus cause a change in k which in turn changes the vibrational motion of the crystal. In practice calculations are done in the Born-Oppenheimer model which is an approximation where the vibrations of the crystal are assumed to be decoupled from the electronic transitions. This is motivated by the fact that the vibrations are very slow compared to the electrons movements. The phonons will then not affect the electronic wave functions but only cause a shift of the electronic levels. See figure 2.6 which also summarizes the previous section. The horizontal distance between the different parabolas is a measure on how much a given electronic transition affects the vibrations of the crystal, or in other words how many phonons that are needed for a transition to take place.

The strength of a transition is proportional to the overlap between the wave functions of the states involved. This is true also in the Born-Oppenheimer picture. Assuming both a low temperature, i.e. $T = 0$ so that only the lowest vibrational level of the ground state is populated and that the two parabolas

are horizontally aligned only a sharp peak will be visible in absorption. This transition is thus described by a vertical arrow between the two lowest vibrational levels. This is a zero-phonon-transition or zero-phonon-line (ZPL). If the parabolas are shifted with respect to one another the overlap will be smaller and for a sufficiently large shift the it will eventually be zero which means that there is no ZPL between the levels.

Since this project was started information has been received indicating the existence of a ZPL in Ce^{3+}:YSO at the wavelength 370.7 nm [11].

Chapter 3

External cavity diode laser

One key component in the planned measurements was a laser diode (LD) from Nichia with a centre wavelength of 372.1 nm at 25 °C. The advantages of using a LD for spectroscopy compared to using a dye laser setup is that the LD is very compact, more stable for day-to-day use and much easier to align. The LD can also easily be tuned by changing the drive current and temperature. There is however one severe limitation with this tuning technique and that is that of mode hopping. This means that it is only possible to tune the laser frequency continuously over a limited region before the frequency changes in a discrete way to some new continuous region. To achieve better scanning characteristics the LD can be placed in an external cavity, this also adds the benefits of single-mode operation and a reduced linewidth. In this section the operation of a LD in an external cavity will be described as well as some relevant theory for LDs in general and blue LDs specifically. For a good introduction on LDs and their use in atomic physics, see [12].

3.1 Theory of laser diodes

A LD is manufactured by growing a thin layer of a p-type material followed by a thin layer of n-type material on a substrate. The two layers form a pn-junction which is called the active layer. By applying a forward bias across the junction electrons are injected into the conduction band of the active layer and holes are injected into the valence band. When holes and electrons are present in the same area they will sooner or later recombine emitting photons at their difference energy. If the electrons and holes can be kept in the same area while only a few electron-hole pairs recombine the photons created will cause stimulated emission. If the forward bias is sufficiently large to inject as many electrons and holes as are lost in the recombination process and if some fraction of the photons created are confined in the active layer, gain will eventually equal losses and laser action will begin.

Although simple, this design isn't very efficient at all. The main problem stems from the fact that the charge carriers aren't confined but can diffuse far out in the p- and n-regions respectively. This decreases the concentration of electron-hole pairs in the active region making the stimulated emission process very weak. There are numerous designs to solve this problem, e.g. double heterostructure lasers and multiple quantum well lasers (MQWL). In the MQWL a very thin layer of a material with a smaller band gap than the surrounding materials have, is sandwiched between the p- and n-layer. This leads to the formation of a well that will force an electron or hole entering to stay there.[1] The different layers will also have different refractive indices. This has the added benefit of making the active layer act as a wave guide further decreasing the optical losses. The light emitted from a LD is almost entirely polarized in the plane of the active layer and shows a large divergence in the plane perpendicular to the active layer giving a characteristic elliptical beam profile if the light is collimated with a lens.

Ever since the first LD was demonstrated, extensive work has been done on creating LDs with larger band gaps giving laser light of shorter wavelengths. The shortest wavelength LDs currently available, are based on GaN-, InGaN- or AlGaN-compounds. They are usually grown on a sapphire substrate in a MQW configuration. Today blue LDs are commercially available at as short wavelengths as 370 nm.[2]

3.2 External cavity diode laser

LDs are extremely sensitive to light coupled back into the LD chip. This can be a problem in practice because unwanted reflections from optical components in an experimental setup can enter the LD and cause both power and frequency instability. But this feature can also be used to improve both the scanning characteristics and the linewidth of the LD. This is the purpose of an external cavity.

[1] The small thickness of this layer causes the charge carriers energy spectrum to become quantized in the direction perpendicular to the layer. The density of states (DOS) for the electrons and holes in the active layer thus reduces from the three-dimensional DOS to the two-dimensional DOS increasing the density of electron-hole pairs at the band gap energy.

[2] The fact that GaN works at all as a LD material is an interesting field of research of itself given the very high impurity concentration in GaN. This fact was actually the main reason to that almost the entire research community had given up on using GaN when building LDs and instead concentrated on ZnS/ZnSe compounds. It was a lone researcher at Nichia Chemicals that moved away from mainstream research and successfully used GaN. The interested reader is referred to [13] which contains both the interesting background story and lots of technical details.

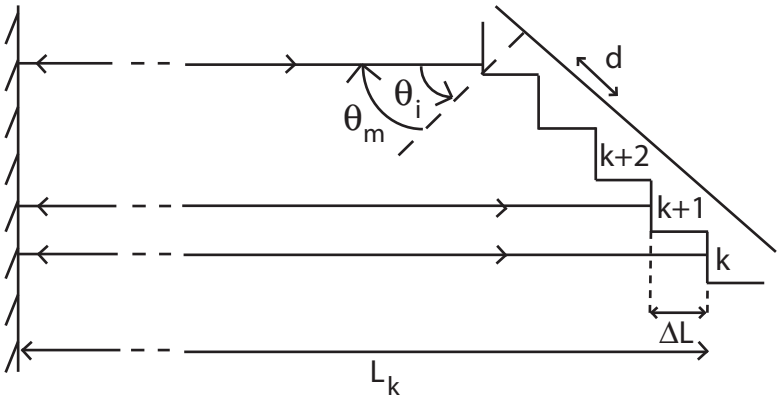

Figure 3.1: Geometry of the grating. L_k is the length of the cavity for a beam being reflected at the kth groove. θ_m is the angle between the grating normal and the reflection order m. θ_i is the angle between the grating normal and the incoming light. d is the distance between the grooves of the grating.

3.2.1 Components of an external cavity

The external cavity design used in this work was a so-called Littrow cavity. It utilizes a grating in the first diffraction order mounted in Littrow configuration as a frequency selective mirror, back-coupling only one specific wavelength into the LD chip. This mode gets a much stronger gain than the modes not being back-coupled into the active layer of the diode and compete favourably with these. The front facet of the LD chip and the grating forms an extended cavity. By changing the angle of the grating, different wavelengths get coupled back and are allowed to lase. The output light consists of the zero order reflection which is not frequency selective.

The wavelength and angles involved are determined by the grating equation:

$$d(\sin\theta_i - \sin\theta_m) = m\lambda. \tag{3.1}$$

Here d is the groove distance, θ_i is the angle of the incoming light relative to the grating normal, θ_m is the angle of the outgoing light of order m relative to the normal and λ is the wavelength of the incoming light. The signs of the two angles are equal on opposite sides of the grating normal.

Since the grating isn't perpendicular to the incoming light, different parts of the beam will experience different cavity lengths. To make the cavity as effective as possible the angle of the grating should be such that the distance between the front facet of the LD chip and every groove should be an integer number times half the laser wavelength. Or in other words:

$$\Delta L = L_k - L_{k+1} = \lambda/2 \tag{3.2}$$

The variables are defined in figure 3.1. From the grating equation it can be seen that this relation is fulfilled when $\theta_i = -\theta_{m=1}$. This angle is given by

$$\theta_i = 90^\circ - \arccos\frac{\Delta L}{d} \tag{3.3}$$

with definitions according to figure 3.1. To change the wavelength inside the cavity the angle of the grating is changed. But a change in wavelength also requires a corresponding change in the external cavity length that is different for every groove.

$$L = \frac{n}{2}\lambda \Rightarrow \frac{dL}{d\lambda} = \frac{n}{2} \Rightarrow \Delta L = \frac{\Delta\lambda}{\lambda}L \tag{3.4}$$

The required change in cavity length to achieve a continuous wavelength scan is thus linear in L. One easy way to accomplish this is to rotate the grating around its pivot point. The pivot point should be located at the crossing between the elongation of the grating arm and the reflecting surface plane of the LD chip.

As mentioned earlier, one of the benefits of using an external cavity is that the linewidth of the laser light decreases. It can be shown that the linewidth of the laser decreases with the length of the cavity, a longer cavity however increases the risk of having multi-mode oscillation [14], partly because of the decreased external cavity longitudinal mode spacing. To ensure single-mode operation it is important to use a grating which is sufficiently frequency selective. Differentiating equation 3.1 with respect to θ_m gives:

$$\Delta\theta_m \sim \frac{m}{d}\frac{1}{\cos\theta_m}\Delta\lambda \equiv \mathcal{D}\Delta\lambda. \tag{3.5}$$

$\mathcal{D}$ is called the linear dispersion of the grating. A large dispersion means that adjacent modes will experience a large deviation which makes them less likely to get a good coupling into the LD chip. Combining equation 3.3 and 3.5 it can be seen that to achieve as large dispersion as possible for a fixed value of λ, d should be as small as possible since

$$\mathcal{D} \sim \frac{1/d}{\cos(90^\circ - \arccos(\lambda/2d))} = \frac{1/d}{\sin(\arccos(\lambda/2d))}.$$

A large dispersion doesn't necessarily mean that two adjacent modes can be resolved. For this to be the case the two modes' reflection maximas from the grating has to be narrow enough not to overlap each other, i.e. the resolution of the grating must be sufficient. The resolution $\mathcal{R}$ is defined as

$$\mathcal{R} \equiv \lambda/\Delta\lambda = mN \tag{3.6}$$

where the last equality holds for a diffraction grating with N illuminated grooves.

Another important property of the grating in the external cavity is the diffraction efficiency defined as:

$$\eta_m = \frac{\text{Power diffracted into order } m}{\text{Power incident on the grating}} \tag{3.7}$$

A large η_1 makes the external cavity modes compete more favourably with the LD modes and also makes it easier to achieve lasing far out in the gain profile of the LD, [15]. However it also reduces the output power of the ECDL since less light is diffracted into the zeroth order. In figure A.1 on page 40 the typical diffraction efficiency in the first order for the grating used in this thesis, is shown for light with S- and P-polarization (S being polarization perpendicular to the grating grooves and P being parallel). In an ECDL the P-configuration is the most common since this will give the largest number of illuminated grooves because of the elliptical beam profile of the light from the LD (the polarization is perpendicular to the major semi-axis of the elliptical beam profile). The P-orientation is also the most efficient configuration in terms of frequency selectivity since the grating will disperse light in the plane perpendicular to the active layer of the LD. This gives a much more selective feedback than dispersion in the plane of the active layer since the active layer is much wider than it's thick ($\sim$ 100 μm compared to $\sim$ 100 nm [15]). Although the curves in figure A.1 seems to suggest that the efficiency can be varied between the values of the S- and P-curves by means of rotating the LD relative to the grating the decreased resolution and frequency selectivity explains why this isn't a good approach. If high output power is required, a better solution would then be to use another grating with a lower efficiency.

3.2.2 Scanning characteristics

To understand the scanning characteristics of the ECDL the transmission profile of the Fabry-Perot etalon formed by the back and front facet of the diode chip needs to be taken into consideration. In figure 3.2 the transmission and gain profiles for all the different components in the ECDL are given. The gain profile of the diode is very broad, typically on the order of nm. In the small interval shown in the figure it can therefore be considered to be constant. As already discussed the grating acts as a frequency selective mirror, deflecting different wavelengths into different directions. This can be modelled as a continuous reflectance curve whose width decreases with increasing resolution and dispersion. The next contribution comes from the longitudinal mode structure of the external cavity. For the cavity used in these experiments the mode-spacing was about $\Delta v = c/2L \approx 10$ GHz with c being the speed of light and $L \approx 1.5$ cm the length of the external cavity. The final transmission profile comes from the etalon formed by the LD itself. Its free spectral range is about 10 times larger than the mode-spacing of the

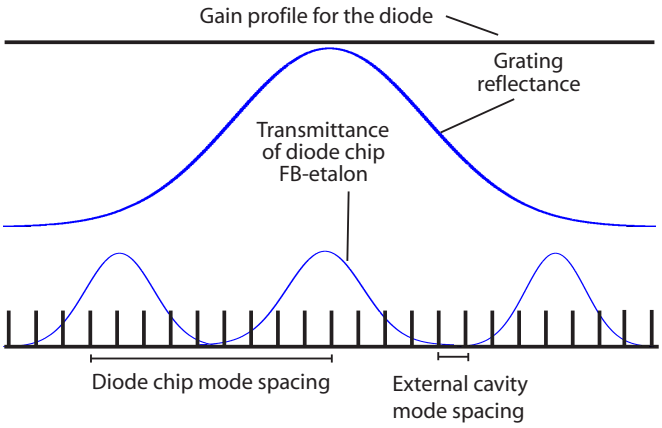

Figure 3.2: The transmission/gain profiles for the different components in the ECDL. (For a 2400 lines/mm grating used at 372.1 nm the grating reflectance curve is more narrow than in the figure.)

external cavity because of the diode chip's shorter length, ~ 0.5 mm. The front facet of the diode typically has a reflectivity R_1 of about ~ 4 % [3] giving a finesse

$$F = \frac{\pi(R_1 R_2)^{1/4}}{1 - \sqrt{R_1 R_2}} \approx 2 \tag{3.8}$$

(or approximately 6 for $R_1 = 0.4$) if R_2 is taken to be 1[4]. From this the width of the transmission peak can be calculated:

$$F = \frac{\Delta v_{fsr}}{\Delta v_{width}} \Rightarrow \Delta v_{width} \approx 50\,\text{GHz} \tag{3.9}$$

assuming $\Delta v_{fsr} = 100$ GHz. Assuming that all these contributions are aligned as in figure 3.2 the lasing will take place at the position of minimal losses. Tilting the grating will correspond to a shift of the grating reflectance curve in the figure eventually making another mode more efficient. But if the length of the cavity is adjusted in conjunction with this rotation (as in the case of rotation around the pivot-point) the external cavity mode

[3] According to [16] the reflectivity is only 4 %. No further reference is given as to why it is so low. In general the reflectivity is given by $(n-1)^2/(n+1)^2$ and assuming $n = 3$ as a rough guess ([17]) for GaN the reflectance should be 25 %. Another article [18] has suggested a reflectivity as high as 40 %. This is however probably an upper bound since Nichia applies a low quality anti-reflection coating on the front facet, [19]. Since no conclusive value has been found, the reflectivity should be regarded as an unknown parameter.

[4] This is usually pretty close to the truth since the back facet often is reflection coated to give the most light in the forward direction of the LD.

structure will move by exactly the same amount as the grating reflectance curve. Because of the broad transmission profile of the diode chip this will allow a continuous scan of the wavelength of within the transmission profile of the diode chip, usually a few tenths of GHz. The scan width can be increased greatly by modulating either the diode temperature or the diode driving current in such a way that also the diode chip mode structure moves by the same amount as the external cavity modes and the grating reflectance curve. Another solution would be to use anti-reflection coated LDs ($R_1 \sim 10^{-5}$) which in the context of figure 3.2 would reduce the diode chip transmission profile to approximately unity for all wavelengths. Both these methods can give scan widths of the order of several tenths of GHz [14, 20] or even nm if used carefully [21].

Chapter 4

Experimental setups and measurements

This work was initially concerned with finding the zero-phonon-line of Ce^{3+} but due to technical difficulties and lack of equipment there was insufficient time to do the actual experiments. The measurements carried out have instead been concerned with testing the components that are planned to be used in the main measurements. Two of the planned setups are still described in this section since they could be useful to anyone continuing on this project and it also makes it easier for the reader to understand the purpose of the different components.

4.1 Equipment

- A Nichia laser diode (NDHU110APAE3) mounted in an external Littrow cavity with a piezoelectric crystal that could be used to fine-tune the grating angle. See appendix A for details on the external cavity.
- A Melles Griot 06DLD103 diode laser driver and temperature controller.
- A Beamlok 2060 cw argon laser used as pump source for the dye laser.
- A Coherent CR-699-21 dye laser and Coherent 7500 Doubler with a LiO_3 frequency doubling crystal (S/N: IN21). Pyridine-2 was used as dye. See appendix B for details on the dye mixing procedure.
- A Michelson interferometer wavelength meter [22].
- A Jobin-Yvon HR1000 High resolution monochromator.
- Two Hamamatsu S1223 photo diodes mounted in 10 kΩ (photo diode A) and 30 kΩ (photo diode B) transimpendance amplifiers.

- A Stanford Research Systems Low noise preamplifier, SR560.
- A Stanford Research Systems Arbitrary Waveform Generator, DS345.
- A New Focus High-voltage amplifier, ν-3211.
- A Fabry-Perot etalon with aluminium mirrors and a number of fixed cavity spacings.

4.2 The external cavity diode laser

A couple of measurements were performed to investigate the characteristics of the laser diode (LD) and to couple it to an external cavity in an efficient way. For details on how to align the ECDL consult appendix A.

4.2.1 Power measurement

Since no dedicated power meter was available at the output wavelength of the LD the laser beam was focused down on a Hamamatsu photo detector mounted in an amplifier with a 10 kΩ transimpendance. The monitor current of the PD mounted behind the LD chip was also registered so that it later could be used to estimate the output power from the ECDL.

4.2.2 Wavelength measurement

When good coupling between the LD and the external cavity had been achieved the beam was directed into the wavemeter. Many attempts to get a reading of the wavelength were made but they all turned out unsuccessful.

Another attempt to measure the wavelength was made using a high resolution monochromator and a CCD camera to register the transmission peaks. To convert the peak position on the CCD coupled to the spectrograph to a wavelength, a calibration spectrum was taken using three peaks from a Hg-lamp. The wavelength of the light from the ECDL was then measured while rotating the grating around the pivot point.

During these measurements two closely spaced peaks were observed at one of the grating angles. The spacing of the two peaks ($\sim$ 0.06 nm) corresponded roughly to the longitudinal mode spacing of the diode chip. At that time it was thought that this was an indication of multi-mode oscillation in the ECDL. Since the separation of the two peaks were at the limits of what the spectrometer could resolve it was realized that the monochromator couldn't be used to analyse the mode structure of the ECDL since the external cavity mode spacing was thought to be even smaller by approximately one order of magnitude, see chapter 3. The problems with measuring the wavelength in the wavemeter could also be related to multi-mode oscillations (see discussion in chapter 5). Since the Ce^{3+}:YSO measurements using the

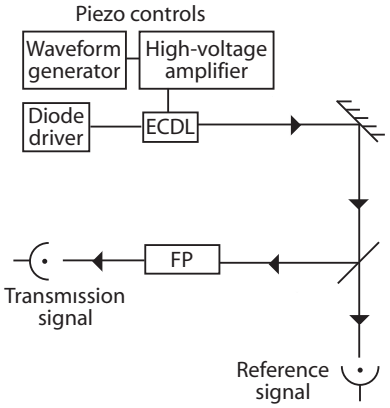

Figure 4.1: Experimental setup for analysing the mode structure of the light from the ECDL.

ECDL required both the wavelength to be measured and single-mode operation it was decided that it was necessary to resolve the mode structure of the ECDL output.

4.2.3 Resolving the mode structure

Lacking equipment to resolve the mode structure the work came to a halt. With only little time remaining on the project a Fabry-Perot etalon (FP) with aluminium mirrors (reflectivity $\sim$ 80 %) and a number of fixed spacers was found. Scanning the wavelength of the ECDL using the function generator and the high-voltage amplifier as a piezoelectric controller, the transmittance of the etalon was measured with photo diode B while monitoring power fluctuations in the ECDL with photo diode A, see figure 4.1. The transmitted light was very weak (probably due to absorption in the thick transparent plates holding the reflecting aluminium layers) so a low noise preamplifier was used to achieve a better signal. The measurements were done for two different etalon lengths, 5 cm and 7 cm. For both of these etalon lengths two different triangular waveforms were applied to the piezoelectric crystal with $V_{peak-to-peak} = 22.4$ V and $V_{peak-to-peak} = 36$ V. The frequency of the triangular waveforms was 5 Hz.

4.2.4 Additional wavelength measurements

The measurements in the previous section indicated single-mode operation of the ECDL. This motivated additional efforts to measure the wavelength using the wavemeter. After some work it was found that the sensitivity of the photo detector (United Detector Technology PIN-020a, according to [22]) used in the wavelength meter was too low around 370 nm, relative to

the noise levels. The detector was replaced with photo detector B and a lens was also inserted into the cavity. After doing this it was noticed that the replaced detector had been AC-coupled and amplified, probably to simplify the fringe counting. To accomplish this the new detector was attached to a low noise preamplifier with high amplification and high-pass filtering. Stable measurements of a 1 mW HeNe beam coupled into the wavemeter required an amplification of approximately 50 times. Despite hard work no fringe pattern appeared. Some time was then spent on measuring the reflectance of the mirrors in the wavemeter cavity as well as measuring the splitting ratio of the beam splitter. The results of the measurements and suggestions on how to simplify wavelength measurements are presented in chapter 5.

4.3 Planned experimental setups

In the beginning of this project the plan was to use the frequency-doubled dye laser system to do the fluorescence measurements that could reveal the existence and position of the ZPL. Therefore more than a month was spent on learning how to operate the dye laser and setting up the frequency doubling system. Since the dye in the laser had to be changed from Rhodamine-6G to Pyridine-2 some time was also spent on mixing the dye and optimizing the concentration (see appendix B). As the dye laser almost was up and running the decision to buy a laser diode and use it for the fluorescence measurements was made. The time invested in setting up the dye laser could have been well spent if it had been possible to measure the wavelength of the light from the ECDL. It would play an important role in measurements after the ZPL had been located.

To make it more clear to the reader how the equipment was to be put into use, two of the planned experiments will now be described.

Locating the ZPL and measuring the linewidth

This setup is concerned with finding the zero-phonon-line (ZPL) of Ce^{3+}. The ZPL is thought to be located at 370.7 nm so the ECDL is tuned from its centre wavelength of 372.1 nm (at $T = 25°$ C) to a wavelength in the vicinity of the ZPL by lowering the temperature of the LD and rotating the grating around the pivot point with the micrometer adjustment screw. To achieve a finer degree of control the piezo-controller is used for the final adjustments. The wavelength is measured by directing a small part of the laser beam into the wavelength meter. The main beam is directed into the cryostat chamber where the Ce^{3+}:YSO is mounted. To account for amplitude variations of the laser beam a reference measurement is made before the cryostat. A number of voltage sweeps with different offsets are applied to the piezoelectric crystal in the ECDL corresponding to a wavelength sweep of a few tenths of a nm, until fluorescence from the ZPL is detected. Once the position of the ZPL

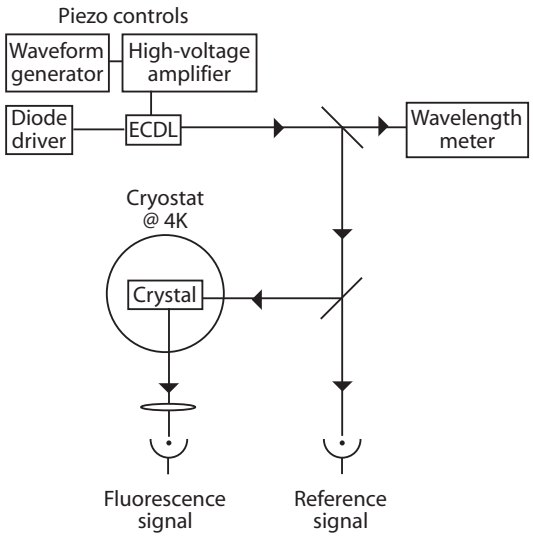

Figure 4.2: Experimental setup for detecting the fluorescence caused by excitation on the ZPL.

is known the linewidth can be found by scanning the ECDL across the ZPL frequency while measuring the transmission as illustrated in the upper part of figure 4.3.

Hole-burning experiments

In this measurement the dye laser is used to burn a hole at the ZPL frequency, see figure 4.3. The light from the dye laser can then switched on and off using an AOM while the transmittance of the ECDL beam can be measured as a function of time. This will reveal how quickly the hole fills up again. Note the use of counter-propagating beams to make sure that the two beams are interacting with the same ions and also to be able to discriminate between the pump beam and the probe beam.

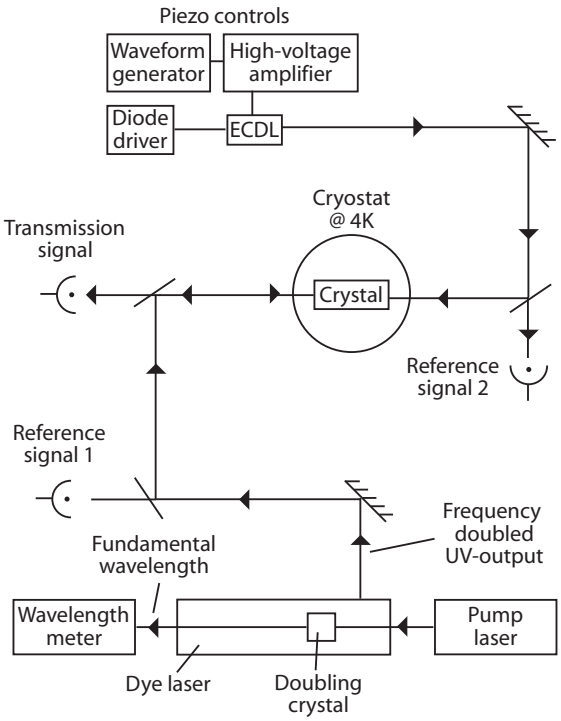

Figure 4.3: Experimental setup for measuring the linewidth of the ZPL (upper half) and doing hole-burning experiments (full setup).

Chapter 5

Results and discussion

5.1 External cavity diode laser

5.1.1 Power measurement

In figure 5.1 the results from the power measurement and the corresponding monitor currents can be seen, both for the LD and the ECDL[1]. Comparison of the two output power measurements show that the threshold current for lasing is $(56.7-49.8)/56.7 \approx 12$ % lower in the ECDL case indicating a good coupling between the LD and the external cavity, [14].

In the specifications from the manufacturer of the LD, a maximum operative monitor current ($I_{max} = 0.251$ mA) is given for the free running diode. Measurements of the first order diffraction efficiency of the grating in the ECDL gave a value of ~ 60 %. Recalling that the reflectivity of the front facet of the laser diode is much smaller (see the discussion in chapter 3) it can be understood that the grating will lead to an increase in the backwards travelling intensity I_4 and in turn also I_2, see figure 5.2. This would seem to change the balance between the intensities I_{out} and I_{mon} compared to the free running laser diode. Following this line of reasoning the maximum monitor current for the LD shouldn't be the same as the maximum monitor current in the ECDL. However, according to [19] the free running monitor current should *not* be exceeded even when the laser diode is in the external cavity, no arguments for this has been given. In figure 5.3 the relation between the output power of the ECDL and the monitor current is shown, indicating a maximum output power of roughly 1.2 mW. This value is much smaller than that from a more naive estimate: $(1 - R_g)P_{LD,max} \approx 0.4 \cdot 20$ mW (see table A.1 on page 41). The small output power is probably related to the large increase in monitor current for the ECDL seen in figure 5.1 but the reasons for this are unknown. Possibly the alignment procedure of the

[1] In the following discussion, LD will refer to the free running laser diode and ECDL will refer to when the laser diode was placed in the external cavity with a good coupling efficiency.

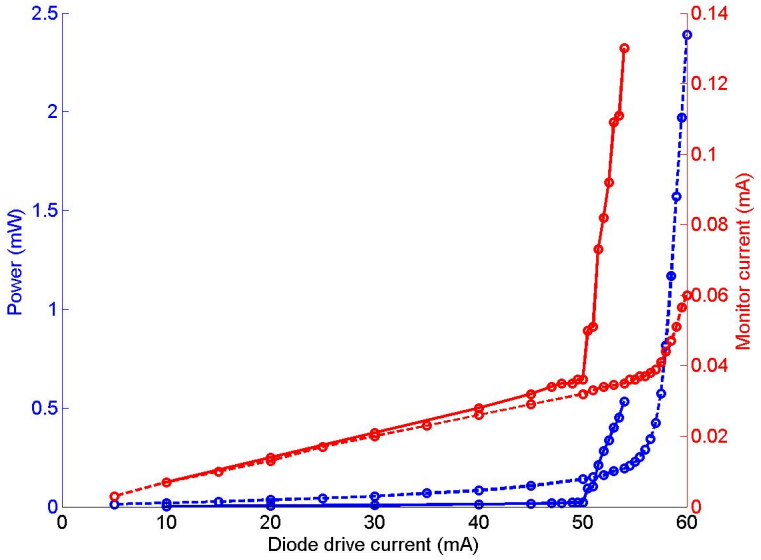

Figure 5.1: Output power (blue lines) and monitor current (red lines) for the LD (dashed lines) and the ECDL (solid lines). The reason for the much larger monitor current for the ECDL is not known.

ECDL should be altered. Summing up, a cautious approach in continued work with the ECDL would be to stay below the maximum monitor current until these issues are better understood.

5.1.2 Wavelength measurements with spectrograph

The results of the wavelength scanning by means of manually rotating the grating while measuring the output light with a spectrograph can be seen in figure 5.4. Four CCD-images are shown where the leftmost peak corresponds to the shortest wavelength achieved by manually rotating the grating. To reach even shorter wavelengths the temperature would have been necessary to adjust. For example, to reach 370.66 nm, the temperature of the LD would have to be lowered to about $13 - 14\,^{\circ}\mathrm{C}$, assuming a temperature coefficient of 0.04 nm/°C. This was below the dew-point in the laboratory where the measurements were done so this could never be tested.[2] The scan width accomplished with the grating however seems large enough though to make it possible to reach the desired wavelength. Here a high efficiency of the

[2]The laboratory where the main experiments were planned to be done was temperature- and humidity-controlled, which would eliminate problems with moist. The spectrograph on the other hand was placed in another laboratory where no such controls were available. Because of practical reasons the spectrograph wasn't moved to the other laboratory.

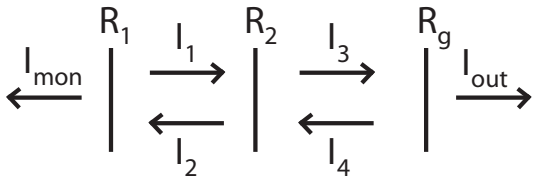

Figure 5.2: A simple model for investigating the intensities in the ECDL. The standing wave character of the light inside the cavity is neglected. I_{mon} is the intensity reaching the internal monitor photo diode behind the laser diode, R_1, R_2 and R_g is the reflectance (or efficiency) of the back facet of the laser diode, the front facet of the laser diode and the grating respectively, I_{out} is the output light from the ECDL.

grating could be beneficial since coupling back much light could make it easier to achieve lasing far out in the gain profile of the LD.

In figure 5.4 one of the CCD-images contains two peaks. The distance between the two peaks is approximately 0.06 nm which would roughly be the longitudinal mode spacing of the laser chip assuming that the length of the active layer in the DL chip is about 0.5 mm and a refractive index of 3 for GaN. The longitudinal mode spacing of the external cavity should be roughly more than one order of magnitude smaller because of the greater length ($\sim$ 1.5 cm) of the external cavity. It then seems very likely that if two or more laser chip modes were allowed to lase at the same time many external cavity modes ($\Delta\lambda \approx 0.005$ nm) also could exist in the cavity at the same time. This shouldn't be taken as more than a guess though since the spectrograph did not have sufficient resolution to resolve the external cavity mode structure. Another plausible explanation for the two peaks could be close competition between the two modes, resulting in fast switching between these, [15].

5.1.3 Resolving the mode structure

In figure 5.5 the results from the Fabry-Perot etalon (FP) measurements can be seen. The time interval shown is equal to one period of a 5 Hz triangular wave, symmetric around $t = 100$ ms. The peaks are transmission maximums of the FP. The irregular distribution and the abrupt changes in transmission are probably due to mode hops in the ECDL. To be able to extract any information from the curves at least two peaks has to be found corresponding to a continuous wavelength scan of the ECDL. As an be seen from the plots this is not a completely obvious choice but an attempt has still been made to analyse the data. The peak spacing is calculated as the average of the spacing between all peak pairs, e.g. $\frac{|a_{-2}-a_{-1}|+|a_2-a_1|}{2}$ for plot **a**. For

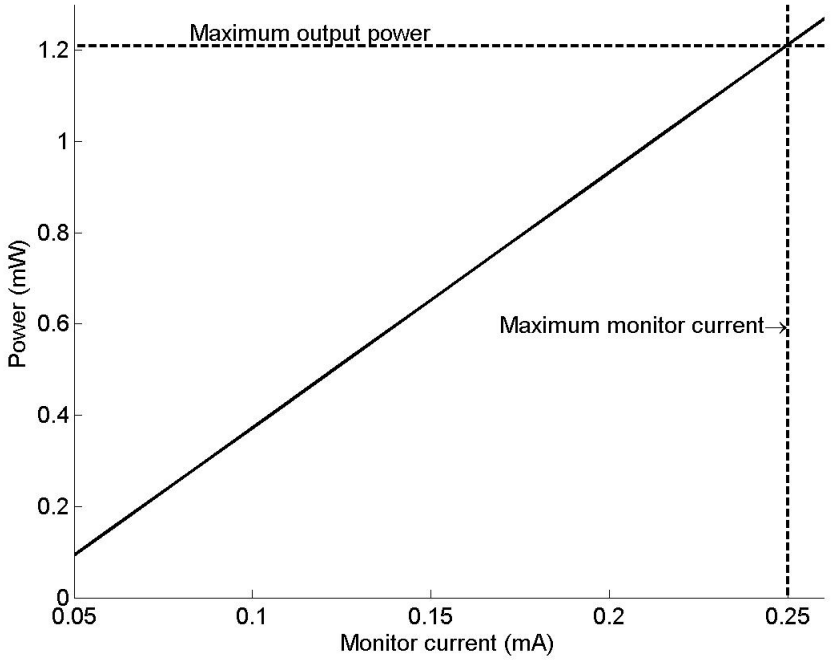

Figure 5.3: Output power from the ECDL as a function of monitor current, extrapolated from the results in figure 5.1. The vertical dashed line shows the maximum allowed monitor current according to the manufacturer of the laser diode.

two transmission measurements with the same FP length the peak spacing should scale inversely as the peak-to-peak values of the applied voltages. For two transmission measurements with different FP length but the same peak-to-peak voltage the peak spacing should be related to each other as the free spectral ranges for the two FP lengths. The results are summarized in table 5.1. The relevant values are then compared in table 5.2. The measured relations are within 10 % of the expected. Although this isn't a close match it seems to suggest that the ECDL is running in single-mode since a multi-mode spectrum probably would give rise to a much more irregular pattern. In the final trace **d** in figure 5.5 it looks like a third transmission peak (d_*) almost is resolved. This indicate a continuous scan-width of at least 4 GHz. Comparison of the spacings $|d_{-4} - d_{-3}| = 11.7$ ms and $|d_{-3} - d_*| = 13.1$ ms seems to indicate some non-linearity in the piezoelectric crystal. This could be an explanation for the discrepancy between the measured and expected values in table 5.1.

There are a number of problems with these measurements. Despite rel-

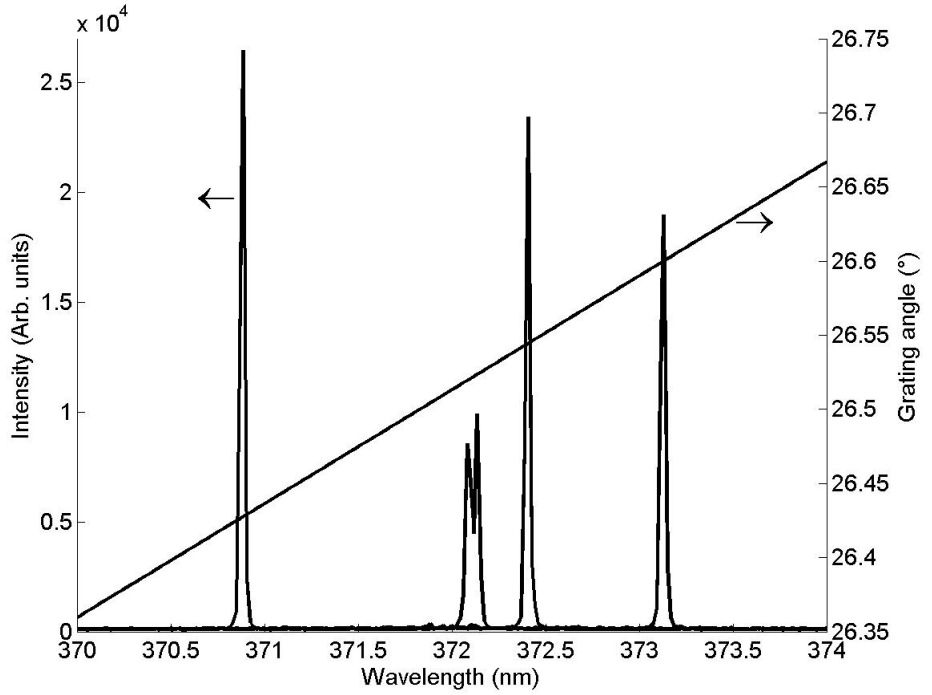

Figure 5.4: Four spectra for a manual wavelength scan by only rotating the grating. The temperature of the laser diode was kept at 25° C. The curve corresponding to the right axis shows the angle of the grating as a function of the wavelength. The angle was calculated from the grating equation (3.1) using $\theta_i = -\theta_m$ with $m = 1$.

atively careful alignment of the FP, zero transmittance was never obtained. This could be due to an irregular beam profile or a slightly divergent beam. This would make the overlap between different reflection orders in the FP non-optimal, thus not making it possible to achieve zero transmittance for the entire beam at the same time. This could also be the reason for the unexpectedly large width of the transmission peaks. The reflectance for aluminium is $\sim$ 80 %, corresponding roughly to a finesse of $F = 15$, which would give a linewidth of $\Delta v_{fsr}/15$. This is clearly not the case in any of the plots in figure 5.5. Another problem is that the FP used was fixed, thus requiring the ECDL to be scanned to show the transmission profile of the FP. Since the continuous scan-width of the ECDL (accomplished by rotating the grating) is unknown, mode hopping could very well take place between the transmission peaks making the conclusions drawn from these measurements invalid. If the FP had been longer, for instance 15 cm, this would give a free spectral range of 0.5 GHz. For an ECDL operating in single-mode this would

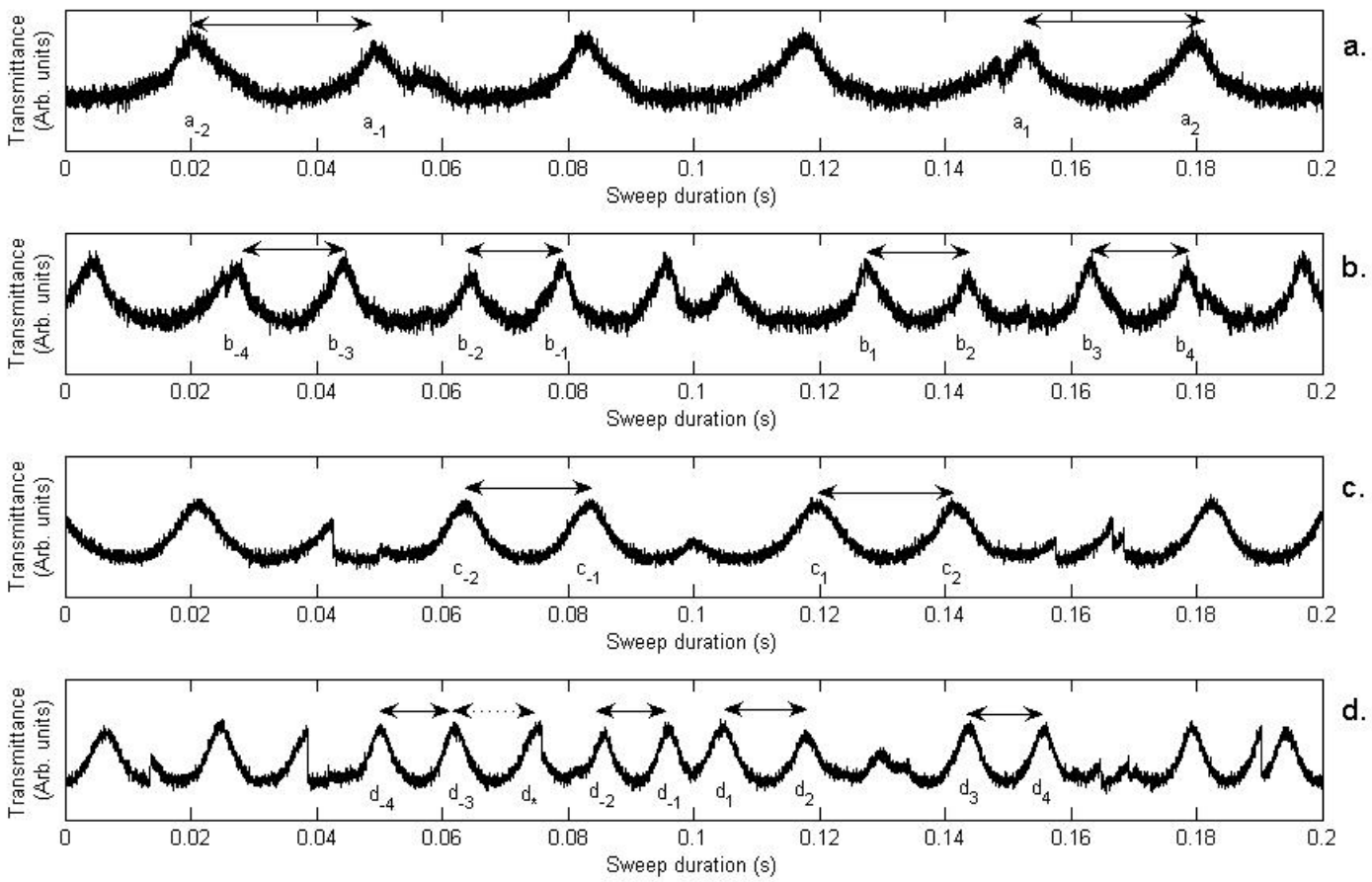

Figure 5.5: Transmission plots of the ECDL beam (for a triangular waveform with peak-to-peak voltage V_{p-p} applied to the piezoelectric crystal) through a Fabry-Perot etalon with free spectral range Δv_{fsr}. **a.** $V_{p-p} = 22.4$ V, $\Delta v_{fsr} = 3$ GHz. **b.** $V_{p-p} = 36.0$ V, $\Delta v_{fsr} = 3$ GHz. **c.** $V_{p-p} = 22.4$ V, $\Delta v_{fsr} = 2.14$ GHz. **d.** $V_{p-p} = 36.0$ V, $\Delta v_{fsr} = 2.14$ GHz.

Plot	**a.**	**b.**	**c.**	**d.**
V_{p-p}	22.4 V	36.0 V	22.4 V	36.0 V
Δv_{fsr}	3 GHz	3 GHz	2.14 GHz	2.14 GHz
Δt	27.6 ms	15.6 ms	20.6 ms	11.7 ms

Table 5.1: The relevant data from the FP transmission measurements. V_{p-p} is the peak-to-peak amplitude of the triangular wave applied to the piezoelectric crystal, Δv_{fsr} is the free spectral range of the FP and Δt is the mean separation of the peak pairs in the respective plots.

Ratios

Expected value	Measured value
$V_{p-p,a}/V_{p-p,b} \approx 0.62$	$\Delta t_b/\Delta t_a \approx 0.57$
$V_{p-p,c}/V_{p-p,d} \approx 0.62$	$\Delta t_d/\Delta t_c \approx 0.57$
$\Delta v_{fsr,a}/\Delta v_{fsr,c} \approx 1.40$	$\Delta t_a/\Delta t_c \approx 1.34$
$\Delta v_{fsr,b}/\Delta v_{fsr,d} \approx 1.40$	$\Delta t_b/\Delta t_d \approx 1.33$

Table 5.2: Relations between the peak spacings and voltage amplitudes and free spectral ranges for the FP. The labels a, b, c, d in the parameter names correspond to the curves in figure 5.5 and the parameter names correspond to the those listed in table 5.1.

probably give at least 5 to 6 equally spaced transmission peaks (depending on the continuous scan-width of the ECDL and disregarding non-linearities in the piezoelectric crystal). This would have been a better way to ensure single-mode operation. An even better method would be to use a scanning FP. The wavelength from the ECDL could then be held fixed while the length of the FP is varied. This would eliminate the risk of mode hopping in the ECDL during measurements and would certainly simplify the analysis.

Even if the ECDL runs in single-mode, it would be interesting to investigate how other gratings with higher groove densities and different diffraction efficiencies would affect the performance. One suggestion would be the Edmund Optics NT-43227 with 3600 lines/mm. This grating also has a lower efficiency at the LD wavelength which could result in an increased power output.

5.1.4 Additional wavelength measurements

Given the great difficulty of measuring the wavelength of the light from the ECDL it seems worthwhile to spend some time on analysing what could be done differently. The wavemeter works by the principle of dividing a reference beam (a HeNe laser with $\lambda_{ref} = 632.816$ nm) into two equal parts using a beam splitter. The two beams then travel through either the left

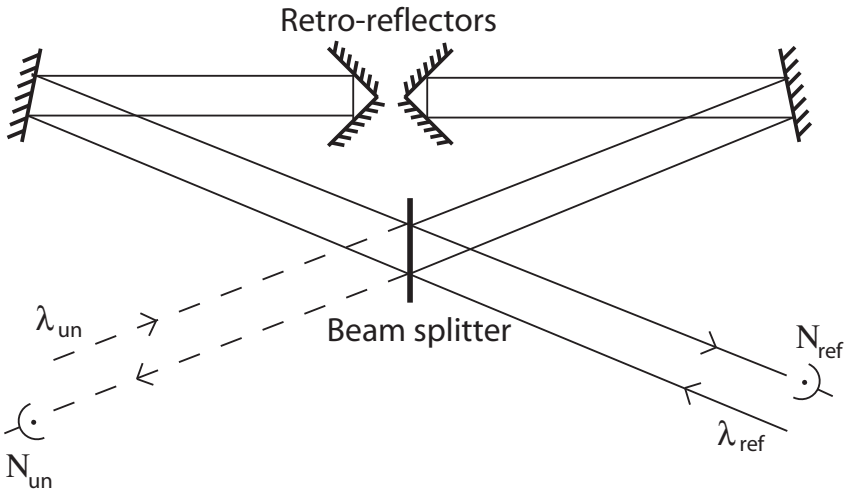

Figure 5.6: Layout of the cavity of the wavemeter used in the experiments. λ_{un} is the wavelength of the beam that is to be measured and N_{un} is the number of fringes it generates at the detector, λ_{ref} is the wavelength of the HeNe reference beam and N_{ref} is the number of fringes it generates at the detector.

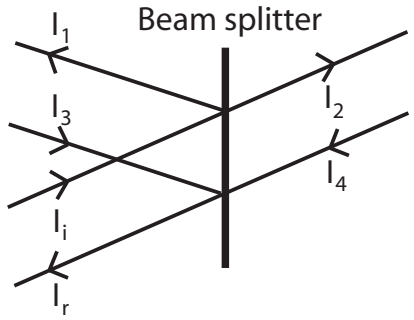

Figure 5.7: The beam-geometry at the beam splitter. I_i is the intensity of the beam whose wavelength is about to be measured. I_r is the intensity of the resulting beam hitting the photo detector.

or right part of the wavemeter cavity, eventually recombining at the beam splitter. The resulting beam is measured using a photo detector, see figure 5.6. If the lengths that the two beams have traversed are different they will have accumulated different amounts of phase and they will therefore interfere constructively or destructively. In the wavemeter this optical path difference (Δx) is varied by moving the retro-reflectors at a constant rate generating a fringe pattern. By counting the number of intensity maximums (N_{ref}) for some interval of Δx and comparing this value with the number (N_{un}) generated by another light source, the unknown wavelength λ_{un} can be calculated.

$$\Delta x = N_{ref}\lambda_{ref} = N_{un}\lambda_{un} \Leftrightarrow \lambda_{un} = \frac{N_{ref}}{N_{un}}\lambda_{ref} \tag{5.1}$$

For a laser running in multi-mode, several frequencies would be present at the same time in the wavemeter. This would result in many interfering fringe patterns at the photo detector, making wavelength measurements impossible.

For the counting procedure to be robust, the fringe pattern must have a sufficient contrast. There are a few factors that decides how good contrast that can be achieved. The most obvious is the overlap between the two interfering beams at the beam splitter and the detector. Another factor is that the angle made by the resulting beam and the normal of the photo detector should be as small as possible. If this angle is large both intensity maximums and minimums could be incident on the detector at the same time. This will result in a constant background intensity in the fringe pattern reducing the contrast. In this wavemeter the angle is non-zero. The third factor is the ratio in which the beam splitter divides the beam into. A beam of intensity I_i hits the beam splitter and is divided into two beams, I_1 and I_2, see figure 5.7. After traversing their respective parts of the wavemeter cavity they recombine at the beam splitter giving a resulting beam of intensity I_r. Neglecting losses in the optical components in the cavity the maximum and minimum value of I_r will be:

$$I_{r,max/min} = (\sqrt{R^2 I_i} \pm \sqrt{T^2 I_i})^2 = (R \pm T)^2 I_i \tag{5.2}$$

The maximum value is not dependent on R and T but the minimum intensity is. For a beam splitter with $R = T$ the largest contrast will be achieved, i.e. $I_{r,max} = I_i$ and $I_{r,min} = 0$. For the reference wavelength the beam was split into almost equal parts ($T \approx 0.6$, $R \approx 0.4$) giving $I_{r,min} \approx 0.04 I_i$. For the ECDL beam the ratio was much more uneven ($T = 0.8$, $R = 0.2$) giving $I_{r,min} \approx 0.36 I_i$ corresponding to a decrease in contrast by almost a factor of 2 compared to the case of $R = T$. This will certainly make the alignment of the wavemeter more difficult not only because of the decreased contrast, but also because it will be very difficult to see the beam that has been reflected twice $R^2 I_i = 0.04 I_i$ and thus make it difficult to overlap

it with $T^2 I_i = 0.64 I_i$. There are also losses inside the wavemeter mainly because of the low reflectivity of the optical mirrors at the LD wavelength. The retro-reflector alone causes a five-fold reduction in intensity and the other mirror reflectivities are ~ 80 %, yielding the intensities $\sim 0.005 I_i$ and $\sim 0.08 I_i$ for the two interfering beams. Although a beam splitter with $R = T$ would improve things ($\sim 0.03 I_i$ for both beams) but the losses would still be high. Given the low reflectivity of the retro-reflectors it doesn't seem unreasonable to be able to replace these with something with maybe 2-3 times higher reflectivity, which would decrease the losses significantly and make the alignment more forgiving for small errors.

Another suggestion that could simplify wavelength measurements is to modify the alignment procedure. The suggested procedure is to carefully align the cavity for the reference beam for a good signal and then to couple in the unknown beam. Since the ECDL beam seems to be much more sensitive to alignment errors than the reference beam it could be advantageous to start and align the cavity for the ECDL beam instead and then couple in the reference beam.

Chapter 6

Conclusions

The single-ion read-out scheme seems very promising in making it possible to construct a single-instance quantum computer instead of using the ensemble approach. However, at the present time it is still unknown if cerium is suitable a read-out ion.

In terms of the initial goals, i.e. locating the ZPL and characterizing it, this project has been a disappointment. It has been *much* more time consuming than expected to setup the external cavity diode laser (ECDL) and especially measuring its wavelength. Also the general lack of usable measurement equipment for wavelengths below 400 nm was unexpected. Good instruments to resolve the mode structure would probably have made the work progress faster. Despite the shortcomings, the ECDL has been aligned and the reduction of the threshold current indicates a good coupling between the laser diode and the external cavity, although the reasons for the low output power are unknown. The scan width accomplished by rotating the grating seems sufficient to tune the ECDL output to the expected ZPL. The attempts to resolve the mode structure of the output from the ECDL indicates single-mode operation although, the results are not conclusive. Wavelength measurements with the wavemeter have not been succesful, probably because of the high losses of the optical componenents in the wavemeter.

Initially the experiments to find the ZPL were planned to be done with a dye laser setup. Knowing the current state of the project it would probably have been wiser to continue with this approach instead of buying the laser diode. In the long run however, the ECDL will probably prove to be a very useful instrument for reading out single qubits.

Despite the hardships the author of this thesis optimistically hopes that his efforts can be of value to anyone continuing on this project, giving a hint on what to do and what not to do.

Chapter 7

Acknowledgements

First I would like to thank my supervisor Stefan Kröll for giving me the opportunity to join the Quantum Information Group for a while. He's been incredibly patient, answering my questions, reading through the manuscript and listening to my never-ending stream of technical problems without showing any signs of growing tired of me. The same goes for my co-supervisor Andreas Wahlter who've maybe had to put up with even more questions and discussions concerning everything from alignment of dye lasers to quantum computing (and a fair share of World of Warcraft).

I would also like to thank the rest of the group Atia Amari, Brian Julsgaard and Lars Rippe for providing a very friendly and nice environment to work in. They've all been very helpful and have always taken their time helping me out and answering my questions.

Also the rest of the people at the Atomic Physics Department deserves thanks for their friendliness. A special thanks goes to Mats Andersson and Linda Persson in the Diode Laser Group for letting me borrow their equipment and use their laboratory, and to Gabriel Somesfalean for answering questions about the ECDL. Anders Persson has also been incredibly helpful in lending me equipment and answering questions about aligning dye lasers although he had absolutely no obligation to help me out.

I'd also like to thank my fellow diploma students for their nice company, especially I'd like to thank my room-mates for the many long and interesting discussions.

Appendix A

Using the external cavity diode laser

A.1 ECDL components

No.	Component	Model
1	Laser diode	Nichia NDHU110APAE3
2	Collimating lens	Geltech C230TM-A
3	Holographic grating	Edmund Scientific 43224
4	Piezoelectric crystal	Physik Instrumente P802.02L
5	Cooling element	Unknown
6	Out coupling mirror	Unknown
7	Laser diode holder screw A	-
8	Laser diode holder screw B	-
9	Collimating lens screw	-
10	Grating block bolt	-
11	Grating micrometer adjustment screw	-
12	Vertical cavity adjustment screws	-
13	Collimating lens adjustment screw	-

Table A.1: Components of the ECDL. Numbers are according to figure A.1

A.2 Aligning the cavity

Inserting the laser diode
Because of the very delicate nature of laser diodes this step should be performed in an ESD safe environment with suitable tools and precautions. Loosen screw 7 and 8 and pull out the diode holder. Pull the white diode

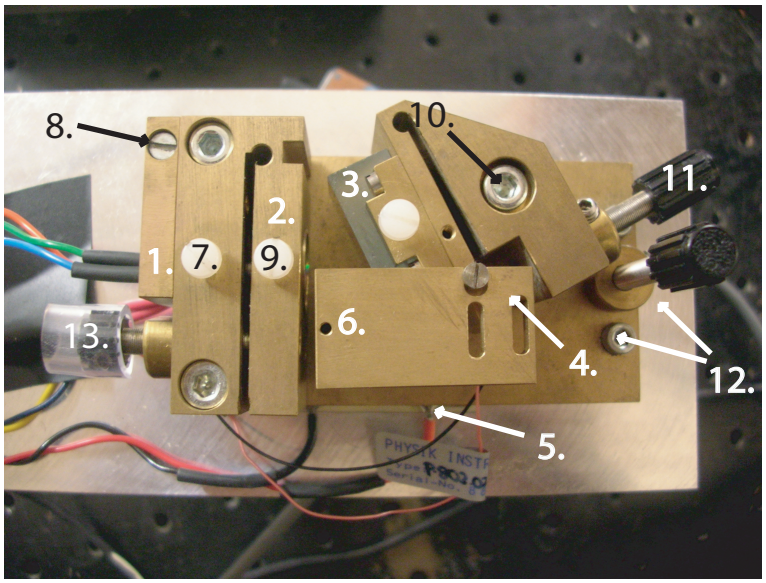

Figure A.1: The external cavity with the mounted laser diode. The number refer to the position of the corresponding item in table A.1.

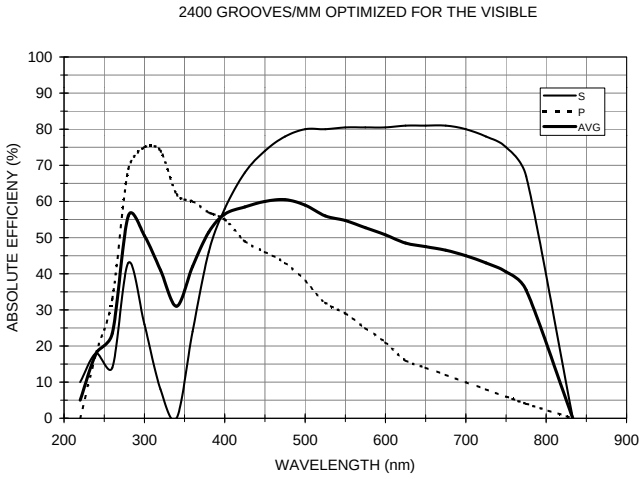

Figure A.2: Typical grating efficiency for polarization parallel and perpendicular to the grooves. (The curves were supplied by the support staff at Edmund Optics.)

Centre wavelength	λ_{center}	372.1 nm
Threshold current	I_{th}	56.7 mA
Operating current	I_{op}	80 mA
Operating voltage	V_{op}	5.05 V
Operating power	P_{op}	20 mW
Operating monitor current	I_{mon}	0.251 mA

Table A.2: Data for the laser diode according to Toptica. The parameters are valid at $T = 25°$ C.

contact out of the metallic cover. Plug the diode into the white contact and put the metallic cover back. Slide the diode holder into the mount and fasten screw 7 and 8.

Collimating the beam

Loosen bolt 10 and remove the grating holding block. Connect the laser to a driver and ramp up the current until lasing begins. Minimize the laser spot size several meters away from the laser by using adjustment screw 13. If a small spot size isn't possible to achieve loosen the collimating lens screw number 9 and carefully move the lens manually in the right direction. Try again to minimize the spot size. It maybe necessary to repeat this process several times before a well-collimated beam is achieved.

Inserting the grating

Adjust the operating current to the laser to just under threshold. Put the grating block back into it's position. Rotate the grating coarsely by hand until two bright spots can be seen on a card outside the cavity. The two spots comes from the zeroth order diffracted beam coming directly from the laser diode and the first order diffracted beam after one round-trip in the cavity respectively. (It might be easier to do this procedure with the out coupling mirror (component 6) removed and instead insert another mirror to couple out the light. This is to avoid the accidental blocking of the cavity light by the edge of the out coupling mirror holder.) Overlap the spots by rotating the grating around the grating bolt axis (component 10) and by using the three vertical adjustment screws, number 12. Once they overlap a sharp increase in intensity and a decrease in threshold current will follow. Fasten bolt 10 and make any necessary fine adjustments with micrometer screw 11. If the out coupling mirror was removed put it back into the cavity.

Note: To minimize the risk of harming the laser diode during this procedure it should be done as far below the free running threshold as possible. Arguments for this are given in chapter 5.

Optimizing the coupling

Reduce the operating current to just below the new threshold current. Make very small adjustments on both screw 11 and 12 until lasing begins. Again reduce the operating current to just below the new threshold and repeat

this procedure until the threshold current has been minimized. It can also be worthwhile to adjust the lens position with screw 13 very slightly. If the initial collimation of the beam isn't good this can give a much better coupling to the external cavity. A good coupling is indicated by a reduction in threshold current of about 10-15 %, [14].

Appendix B

Pyredine-2 dye mixing procedure

1. Solve 1 gram Pyridine-2 in 50 ml ethanol.
2. Directly add 50 ml ethylene-glycol.
3. Pour 900 ml ethylene-glycol into the dye-pump.
4. Pour 50 ml of the dye-solution into the dye-pump.
5. Repeat a-c until power stops to increase.
   (a) Add small amounts of dye-solution to the system.
   (b) Get system to lase.
   (c) Maximize for power.

The results for the dye used in the experiments can be seen in the table and figure below. The dye optimization procedure was done with the laser operating in the CR-699-01 configuration, i.e. without the ICA and galvo-plate, with the Lyot-filter rotated to $\lambda = 725.1$ nm.

Solution (ml)	Concentration dye powder (g / l)	Power (mW)
50	0.53	-
60	0.63	300
63	0.65	340
66	0.68	380
69	0.71	400
72	0.74	420
75	0.77	420

Table B.1: Measured output powers for different amounts of Pyredine-2 dye.

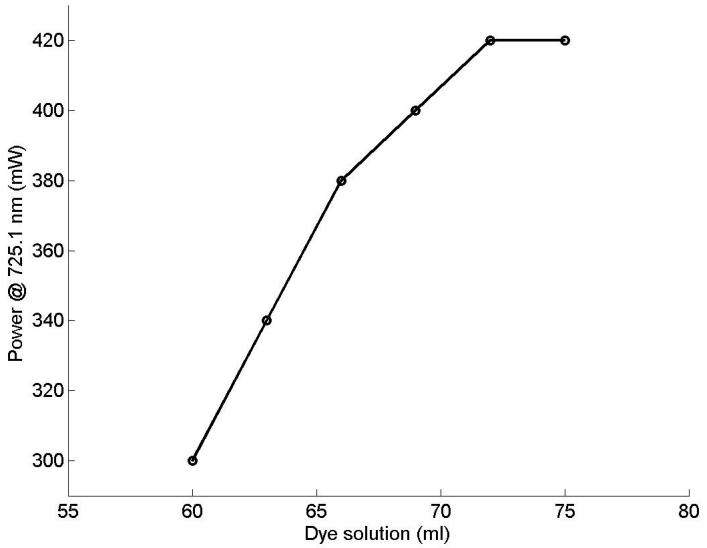

Note: After the final addition of solution it was noted that some unsolved dye powder was left at the bottom of the measurement cup. Therefore the final amounts of solution added could have contained less dye powder than the first ones. So the concentrations should only be used as a rough estimate.

Bibliography

[1] Michael A. Nielsen and Isaac L. Chuang. *Quantum Computation and Quantum Information*. Cambridge University Press, 2000.

[2] Richard Feynman. Simulating physics with computers. *International Journal of Theoretical Physics*, 21(6–7):467–488, 1982.

[3] David Deutsch. Quantum theory, the Church-Turing principle and the universal quantum computer. *Proceedings of the Royal Society of London. Series A, Mathematical and Physical Sciences*, 400:97–117, 1985.

[4] Peter W. Shor. Polynomial-time algorithms for prime factorization and discrete logarithms on a quantum computer. *arXiv:quant-ph*, 9508027, January 1996.

[5] Lov K. Grover. A fast quantum mechanical algorithm for database search. *arXiv:quant-ph*, 9605043, May 1996.

[6] C. Negrevergne, T. S. Mahesh, C. A. Ryan, M. Ditty, F. Cyr-Racine, W. Power, N. Boulant, T. Havel, D. G. Cory, , and R. Laflamme. Benchmarking quantum control methods on a 12-qubit system. *Physical Review Letters*, 96(17):170501, 2006.

[7] Mattias Nilsson. *Coherent Interactions in Rare-Earth-Ion-Doped Crystals for Applications in Quantum Information Science, LRAP-333*. PhD thesis, Lund Institute of Technology, 2004.

[8] Janus H. Wesenberg, Klaus Mølmer, Lars Rippe, and Stefan Kröll. Scalable designs for quantum computing with rare-earth-ion-doped crystals. *arXiv:quant-ph*, 0601141, January 2006.

[9] R.S. Meltzer and S.P. Feofilov. Spectral hole burning in the 4f-5d transitions of Ce^{3+} in $LuPO_4$ and YPO_4. *Journal of Luminescence*, 102–103:151–155, 2003.

[10] B. Henderson and G.G. Imbusch. *Optical Spectroscopy of Inorganic Solids*. Oxford University Press, 1989.

[11] Unpublished absorption measurement on Ce^{3+}:YSO done by Philippe Goldner at Laboratoire de Chimie de la Matière Condensée de Paris in March 2006.

[12] Carl E. Wieman and Leo Hollberg. Using diode lasers for atomic physics. *Review of Scientific Instruments*, 62:1–20, January 1991.

[13] Shuji Nakamura, Stephen Pearton, and Gerhard Fasol. *The blue laser diode - The complete story.* Springer, 2nd edition, 2000.

[14] L. Ricci, M. Weidemüller, T. Esslinger, A. Hemmerich, C. Zimmermann, V. Vuletic, W. König, and T.W. Hänsch. A compact grating-stabilized diode laser system for atomic physics. *Optics Communications*, 117:541–549, 1995.

[15] D J Lonsdale, A P Willis, and T A King. Extended tuning and single-mode operation of an anti-reflection-coated ingan violet laser diode in a littrow cavity. *Measurement science and technology*, 13:488–493, 2002.

[16] Johan Hult, Iain S. Burns, and Clemens F. Kaminiski. Wide-bandwidth mode-hop-free tuning of extended-cavity GaN diode lasers. *Applied Optics*, 44(18):3675–3685, 2005.

[17] N. A. Sanford, L. H. Robins, A.V. Davydov, A. Shapiro, D.V. Tsvetkov, and A. V. Dmitriev. Refractive index study of $Al_xGa_{1-x}N$ films grown on sapphire substrates. *Journal of applied physics*, 94(5):2980–2991, 2003.

[18] Lars Hildebrandt, Richared Knispel, and Joachim R. Sacher. Robust external cavity diode lasers with implemented antireflection coated blue laser diodes and their performance in atom absorption spectroscopy. Article found on www.sacher-laser.com - Sacher Lasertechnik.

[19] Mail correspondance with Anselm Deninger – Product manager at Toptica Photonics AG.

[20] Lars Hildebrandt, Richard Knispel, Sandra Stry, Joachim R. Sacher, and Frank Schael. Antireflection-coated blue gan laser diodes in an external cavity and doppler-free indium absorption spectroscopy. *Applied Optics*, 42(12):2110–2118, 2003.

[21] D. Wandt, M. Laschek, K. Przyklenk, A. Tünnermann, and H. Welling. External cavity laser diode with 40 nm continuous tuning range around 825 nm. *Optics Communications*, 130:81–84, 1996.

[22] Hans Hertz and Lars-Åke Nilsson. Konstruktion och testning av digital våglängdsmätare. Master's thesis, Lund Institute of Technology, 1980.